Alkylation on Solid Acids. Part 2. Single-Event Kinetic Modeling

Jorge M. Martinis[†] and Gilbert F. Froment*

Artie McFerrin Department of Chemical Engineering, Texas A & M University, College Station, Texas 77843-3122

The reaction network of isobutane alkylation with butenes over proton-exchanged Y-zeolites was generated at the elementary-step level of carbenium-ion chemistry by means of the Boolean relation matrix approach. A significant reduction in the number of model parameters from 3130 to 14 was accomplished by expressing elementary-step rate coefficients in terms of the single-event concept together with the application of the Evans−Polanyi relationship, the stabilization energy concept, and thermodynamic constraints. The deactivation was expressed in terms of site coverage by higher oligomers. For parameter estimation, the complete kinetic model was embedded into a model for the fixed-bed reactor used in the experimental investigation. Nonlinear regression led to parameter values in line with the rules of carbenium-ion chemistry. The simulation of the transient behavior of the fixed-bed reactor illustrates how deactivation occurs in a narrow zone moving through the catalyst bed leading to a typical breakthrough in the product composition with process-time.

Modeling Deactivation through Site Coverage

Part 1 of this investigation reported on an extensive experimental program comprising 135 data sets collected during nine runs with different butene space-times and temperatures.

In alkylation of isobutane with butenes over proton-exchanged zeolites, transformations at the elementary-step level involve either one or two Brönsted acid sites, which are assumed to be distributed over the catalyst with uniform strength. A set of eight types of elementary steps was identified as the most likely transformations occurring within the reaction network at the acidity and temperature range of interest.[1]

Whereas oligomerization to higher olefins is a relatively rapid process on acid catalysts,[2,3] GC/MS analyses of the reactor exit flow reveal that, on an isobutane-free basis, C_9+ species accounted for <1% of the total peak area. Thus, the absence of C_9+ species in the product is a strong indication that deactivation can be a direct consequence of the formation of C_9+ species irreversibly adsorbed on acid sites, i.e., to irreversible site coverage.

The cation exchange capacity (CEC) of a Zeolyst CBV600 protonated Y-zeolite with estimated formula $H^+_{58}(AlO_2^-)_{58}$-$(SiO_2)_{150}\cdot 240H_2O$ is calculated to have a value of 3.46 mol/gCat (C^t_{H+}). The total concentration of acid sites (C^t_{H+}) is then detailed as the sum of the concentration of free acid sites (C_{H+}) and of the concentrations and of those reversibly (C_{Rn+}) and irreversibly (C_{Rm+}) covered:

$$C^t_{H+} = C_{H+} + \sum_{n=1}^{N} C_{R_n^+} + \sum_{m=1}^{M} C_{R_m^+} \qquad (1)$$

The reaction network contains 78 ions (N) that reversibly adsorb and 541 ions (M) that irreversibly adsorb. Considering all C_9+ ions as irreversibly adsorbed does not impair their reaction via other elementary steps. The experimental observation of a nonzero steady butene conversion strongly suggests that nonnegligible amounts of irreversibly adsorbed material react via β-scission toward equilibrium with lower oligomers. A detailed account of the fate of each species present on the catalyst surface is required to account for this process.

For site coverage, the point value of the deactivation function can be written as $1 - \theta_{irr}$, whereas the concentration of free acid sites (C_{H+}) can be written in terms of the reversible fractional site coverage (θ_{rev}) and the deactivation function (φ):

$$\varphi = 1 - \theta_{irr} = 1 - \sum_{m=1}^{M} (C_{R_m^+}/C^t_{H+}) \qquad (2)$$

$$(C_{H+}/C^t_{H+}) = \varphi(1 + \sum_{n=1}^{N} (C_{R_n^+}/C_{H+}))^{-1} = (\varphi/1 + \theta_{rev}) \qquad (3)$$

Equation 2 postulates that the deactivation function varies linearly with the irreversible fractional site coverage; however, if more than one acid site is required for a particular type of elementary step, higher orders may be necessary as derived by Nam and Froment.[4] It should be emphasized here that the deactivation is expressed rigorously in terms of the amount of covered sites and not empirically in terms of process-time.

Rate-Controlling Steps and Liquid Sorption in Zeolites

Among all the elementary steps considered, alkene (de)-protonation and hydride transfer turn out to be the only interactions occurring between a molecule from the fluid phase and an acid site. They act as initiation or termination steps, whereas all the other elementary steps involve transformations among surface-bonded carbenium ions exclusively. The (de)-protonation elementary steps are intrinsically much faster than those involving surface-bonded ions and, therefore, reach pseudo-equilibrium. The surface concentrations of intermediate ions (C_{Rn+}) are related to liquid-phase concentrations of sorbed alkenes inside zeolite cages, (C^s_i), by means of state functions:

$$C_{R_n^+} = K_p(R_i^=;R_n^+)\frac{C_i^s C_{H+}}{C^\circ} = K_p(R_i^=;R_n^+)\left(\frac{V_L}{V_p}\right)C_i^s C^t_{H+}\left(\frac{1-\theta_{irr}}{1+\theta_{rev}}\right) \qquad (4)$$

The temperature-dependent protonation equilibrium constant (K_p) can be directly related to the change of the Gibbs free energy upon reaction:

* Corresponding author e-mail: g.froment@chemail.tamu.edu.

[†] Present address: PDVSA INTEVEP, Urb. Santa Rosa, Sector El Tambor, Los Teques, Venezuela. Current e-mail: martinisj@aggienetwork.com.

10.1021/ie050910v CCC: $33.50
Published on Web 01/07/2006

$$\left[\frac{C_{R_{n^+}}C^\circ}{C_i^s C_{H+}}\right] = K_p(R_i^=;R_n^+) = \exp\left(-\frac{\Delta G_p}{RT}\right) \quad (5)$$

The concentration of the pure liquid ($C°$) shows up in eq 4 because the standard state of the liquid reactant is different from unity. To obtain the value of $C°$ in engineering units, like mol/gCat, the inverse value of the standard molar volume for the pure liquid, (V_L), together with the catalyst pore volume (V_p), are used. Calculation pathways from pure components in the perfect gas state at standard conditions to the liquid mixture assume ideal solution and negligible pressure effects because, at the reaction temperature, the total pressure (35 bar) is much higher than the vapor pressures for all the species present in the liquid phase.

The liquid-phase concentration of the sorbed ith alkene inside the zeolite cannot be measured directly, and therefore, it is expressed in terms of the accessible liquid bulk concentration (C_{Ri+}):

$$C_{R_i^=}{}^s = K_s C_{R_i^=} = \bar{C}_{sat}\left(\frac{V_L}{V_p}\right)C_i = \bar{C}_{sat}x_{R_i^=} \quad (6)$$

Given the high dilution of the mixture components in isobutane and assuming that the zeolite cages are filled with liquid, a unique value is taken for the sorption partition coefficient K_s of the alkene species, in accordance with the results of Denayer et al.,[5] who studied the liquid-phase hydroconversion of a heptane/nonane mixture over a Pt-USY zeolite. Assuming saturation inside the zeolite cages, the sorption partition coefficient leads to an average saturation concentration for all species considered.

The surface concentration of the reaction intermediates is related to quantities that can be estimated from thermodynamics as well as to the accessible molar fractions of the species in the liquid bulk ($x_{Ri=}$):

$$C_{R_{n^+}} = K_p(R_i^=;R_n^+)\left(\frac{V_L}{V_p}\right)\bar{C}_{sat}x_{R_n=}C_{H+}^t\left(\frac{\varphi}{1+\theta_{rev}}\right) \quad (7)$$

Equation 7 can also be used to express the reversible fractional site coverage as a function of the molar fractions in the liquid bulk:

$$\theta_{rev} = \sum_{n=1}^{N}\frac{C_{R_{n^+}}}{C_{H+}^t} = \sum_{n=1}^{N}K_p(R_i^=;R_n^+)\left(\frac{V_L}{V_p}\right)\bar{C}_{sat}x_{R_i^=} \quad (8)$$

The deactivation model needs to be introduced into the rate equations of the process.

Rate Equations at the Elementary-Step Level

As mentioned in Part 1, the reaction network generated from only two feed molecules and eight different types of carbenium-ion elementary steps led to 3130 elementary steps among 753 species. A significant reduction of the number of independent parameters is possible by accounting for equilibrium relationships. Thus, rates for 294 (de)protonation elementary steps are replaced by their corresponding equilibrium relationships by means of eq 5. Equilibrium is set for all possible adsorption/desorption interactions among the 134 molecules present in the liquid phase and the 78 reversibly adsorbed ions serving as intermediates in surface elementary steps.

The surface elementary steps comprise 2836 transformations among surface-bonded carbenium ions. In what follows, rate expressions for every surface elementary step are formulated according to the principles of the transition-state theory (TST), stating that, for an elementary step, reactants are in equilibrium with the transition state. TST also states that the reaction rate of an elementary step depends on an intensive measure of the amount of each reactant raised to the absolute value of its stoichiometric coefficient, a direct consequence of the application of the principle of microscopic reversibility. This principle establishes that the transition state for a given reaction and its reverse must be the same. Upon the application of the TST to the definition of the reaction rate of an elementary step, three different types of rate expressions can be written for the six types of elementary steps considered.

For all monomolecular steps (β-scission, PCP branching, methyl-shift, and hydride shift), the rates can be written, explicitly accounting for the deactivation:

$$r_j = k_j' C_{R_n}{}^+ = k_j' K_p(R_i^=;R_n^+)\left(\frac{V_L}{V_p}\right)\bar{C}_{sat}C_{H+}^t\left(\frac{\varphi}{1+\theta_{rev}}\right)xR_i^= \quad (9)$$

$$r_j = k_j' C_{R_{m^+}} \quad (10)$$

In the particular case of the transformations involving reversibly adsorbed ions, eq 9 allows rewriting the reaction rate as a function of the liquid bulk composition, whereas elementary steps involving irreversibly adsorbed species have to be written in terms of their local surface concentrations.

Reaction rates for bimolecular elementary steps (oligomerization and hydride transfer) occurring over single acid sites are directly formulated in terms of the liquid-phase concentration of the sorbed reactant (C_o^s or C_p^s):

$$r_j = k_j' C_{R_n}{}^+ C_o{}^s = k_j' K_p(R_i^=;R_n^+)\left(\frac{V_L}{V_p}\right)\bar{C}_{sat}{}^2 C_{H+}^t\left(\frac{\varphi}{1+\theta_{rev}}\right)x_{R_i=}x_{R=} \quad (11)$$

$$r_j = k_j' C_{R_{n^+}} C_p{}^s = k_j' K_p(R_i^=;R_n^+)\left(\frac{V_L}{V_p}\right)\bar{C}_{sat}{}^2 C_{H+}^t((\varphi^2/1+\theta_{rev}))xR_i^=x_R \quad (12)$$

Notice that, in both eqs 11 and 12, only reversibly adsorbed carbenium ions appear as reactants. For any irreversibly adsorbed ion, bimolecular elementary steps would result in model-forbidden outcomes such as desorption of a C_9+ ion by hydride transfer or the formation of a $C_{13}+$ irreversibly adsorbed ion.

The rate equation (eq 12) for hydride transfer contains a different type of deactivation function (φ^2) to account for the effect of a weak but real interaction between the reacting alkane and a neighboring acid site. This interaction, first identified through quantum chemical calculations by Kazansky,[6] does not imply adsorption or occupancy of the acid site by the alkane and, therefore, does not affect the fractional site coverage of acid sites. Yet, this latter quantity significantly determines the hydride-transfer activity by reducing, to a large extent, the availability of neighboring acid sites. A stochastic description of single- and dual-site reaction mechanisms for deactivating reaction sets can be found in the paper by Nam and Froment.[4] On the basis of results for the case where main reactions occur on dual sites and deactivation reactions occur on single sites, a deactivation function involving a quadratic dependency on the

irreversible fractional site coverage is proposed in the present model for the hydride-transfer step.

Clearly, a kinetic model comprising ~2836 rate coefficients makes it untractable or even useless for practical purposes. It would also require an unrealistic amount of experimental data. The concept of single event provides the means for a drastic reduction in the number of independent kinetic parameters.

Single-Event Concept

First introduced by Froment and co-workers,[7,8] the single-event concept is based on the fundamental framework of TST. This concept factors the structural contributions associated with a single elementary step out of the TST rate coefficient. The number of distinct configurations taken by a reactant and its transition state is related to changes in their symmetry numbers to account for all possible occurrences of identical single events making up the elementary step. The TST equation for the rate coefficient contains the vibration frequency along the reaction coordinate converted to a translation that leads the passage from the transition state to products ($\Lambda = k_B T/h$) and followed by the reactant−transition-state equilibrium constant ($K^{\ddagger}$) which is further split into the reactant−transition-state entropy change ($\Delta S^{\circ\ddagger}$) and the energy barrier ($\Delta H^{\circ\ddagger}$).

$$k' = \Lambda K^{\ddagger} = \left(\frac{k_B T}{h}\right) \exp\left(\frac{\Delta S^{\circ\ddagger}}{R}\right) \exp\left(-\frac{\Delta H^{\circ\ddagger}}{RT}\right) \qquad (13)$$

Separation of structural effects associated with symmetry changes between the reactant and the transition state from the structure-independent intrinsic entropy change ($\Delta \hat{S}^{\circ}$) leads to a unique value for all possible single events within a given elementary step:

$$\Delta S^{\circ\ddagger} = \Delta \hat{S}^{\circ} + R \ln\left(\frac{\sigma_{gl}}{\sigma_{gl}^{\ddagger}}\right) \qquad (14)$$

By combining eqs 13 and 14, structural effects associated with distinct single events of an elementary step are factored out of the rate coefficient:

$$k' = \Lambda \exp\left(\frac{\Delta \hat{S}^{\circ}}{R}\right)\left(\frac{\sigma_{gl}}{\sigma_{gl}^{\ddagger}}\right) \exp\left(-\frac{\Delta H^{\circ\ddagger}}{RT}\right) \qquad (15)$$

The ratio of the global symmetry number of the reactant molecule (σ_{gl}) to the global symmetry number of the transition state ($\sigma_{gl}^{\ddagger}$) is defined as the number of single events (n_e):

$$n_e = \frac{\sigma_{gl}}{\sigma_{gl}^{\ddagger}} \qquad (16)$$

As a result, the rate coefficient of an elementary step (k_j') is a multiple of the single-event rate coefficient in such a way that only those structural effects associated with the stability of the carbenium ions remain present. Hence, eq 17 sets the single-event rate coefficient as a function of the surface-bonded carbenium-ion types present (t_{Rr+}, t_{Rp+}).

$$k_j' = n_e \tilde{t} k_j(t_{R_r^+}; t_{R_p^+}) \qquad (17)$$

The introduction of the single-event concept allows a drastic reduction in the number of model parameters. By grouping the vibration frequency along the reaction coordinate and the intrinsic entropy change, a single, structure-independent frequency factor $\tilde{A}$ is obtained per type of elementary step. All the remaining structure-dependent contributions associated with a particular elementary step end up inside the energy barrier. The latter can be approximated by the energy of activation of the elementary step occurring in the liquid phase ($E_a \approx \Delta H^{\circ\ddagger}$, J/mol) so that an Arrhenius-like expression is obtained for the single-event rate coefficient:

$$\tilde{k}_j(t_{R_r^+}; t_{R_p^+}) = \left[\Lambda \exp\left(\frac{\Delta \hat{S}^{\circ}}{R}\right)\right] \exp\left(-\frac{\Delta H_j^{\circ\ddagger}}{RT}\right) = \tilde{A}_{\text{ElemStepType}} \exp\left(-\frac{E_{aj}}{RT}\right) \qquad (18)$$

The number of frequency factors is now reduced from 2836 to 6, i.e., only 1 per type of elementary step.

Calculation of the Number of Single Events

The application of the single-event concept requires the number of single events for each elementary step, as defined by eq 16. The calculation starts with the numerical representation of the molecule or ion by a Boolean matrix.[8] The external symmetry number, which corresponds to the number of indistinguishable configurations of the molecule considered as a rigid rotor, is calculated from the molecular topology using the methodology described by Muller et al.[9] and by Walters and Yalkowsky.[10] The method is based on the identification of the centers of symmetry by recursively removing layers of atoms. Simple rules applied to each layer yield contributions to the external symmetry number (σ_{ext}) that depend on the hybridization state (sp^2 or sp^3) of each carbon atom. The identification of two- and three-fold internal symmetry axes (n', n'') and chiral centers (n''') within the structure is necessary to determine additional contributions to the global symmetry number, as indicated in eq 19.

$$\sigma_{gl} = \sigma_{ext} \frac{2^{n'} 3^{n''}}{2^{n'''}} \qquad (19)$$

The applicability of this method is limited to acyclic hydrocarbon structures, where information on hindered internal rotations is not relevant.

In general, the pathway from reactants to transition states along the reaction coordinate involves the creation and/or destruction of symmetry axes and chiral centers by changing the bond distances and positions of the carbon atoms in the α- and/or β-position with respect to the one that carries the positive charge or is part of a double bond. This process of creating and/or destroying symmetry axes and chiral centers determines the number of single events for a given elementary step. Table 1 illustrates this process for both monomolecular and bimolecular elementary steps considered in the present model. The appearance or disappearance of two- and three-fold symmetry axes and/or chiral centers is indicated by changes to the global symmetry number in multiples of two or three.

The validity of transformations occurring in surface-bonded carbenium-ion structures on those in free-carbenium structures may be questionable. However, Park and Froment[11] studied the effect of the surface bonding of carbenium ions and concluded that both the reactant and the transition state undergo similar reductions in their global symmetry numbers with surface bonding. Consequently, the ratio (eq 16), i.e., the number of single events, is the same for both cases.

Park and Froment[11] also validated the independence of the single-event frequency factor with respect to the molecular

Table 1. Examples of Symmetry Transformations in Elementary Steps[a]

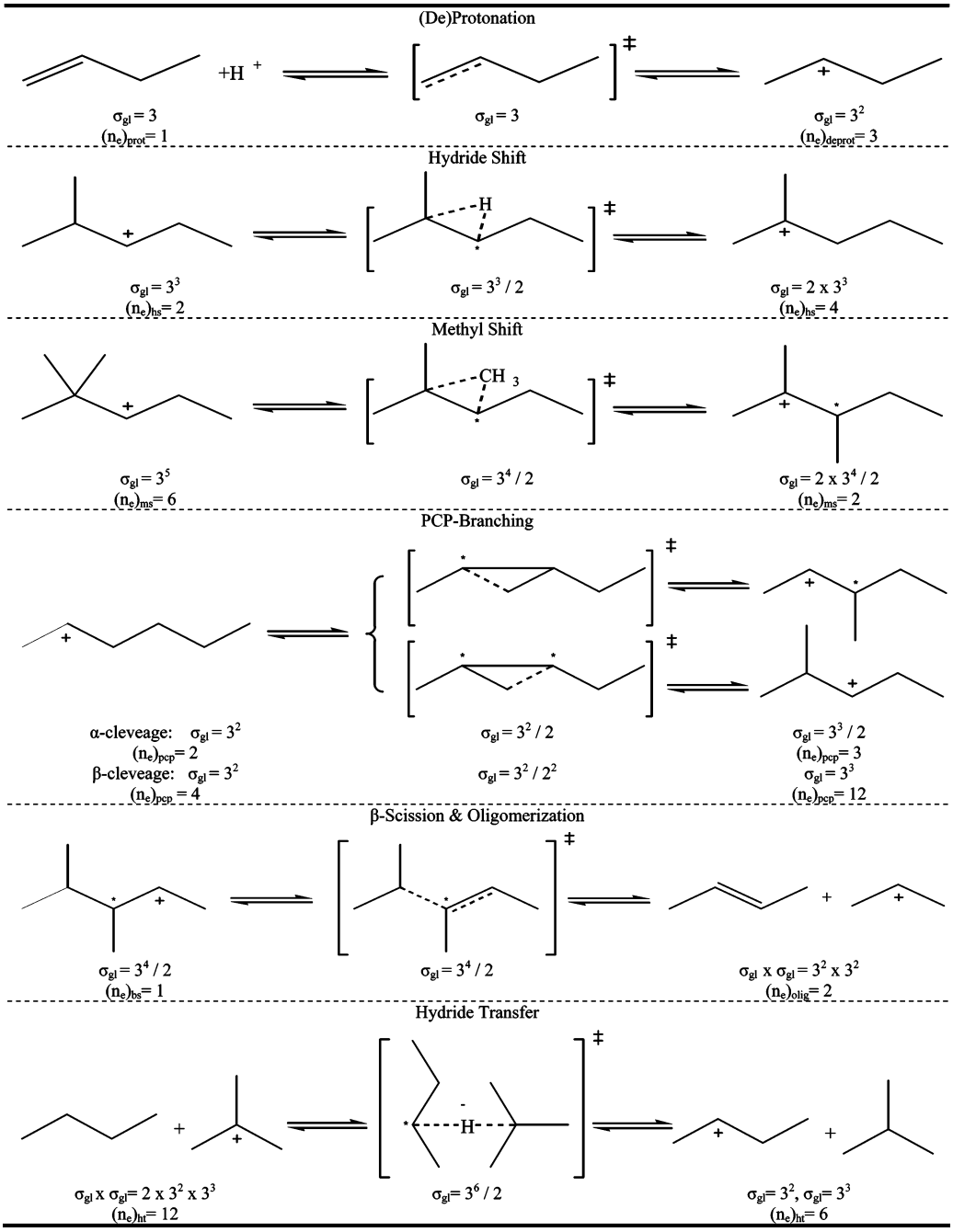

[a] Dotted lines = variable length bonds; double dagger = transition-state structures; and asterisk = position of a chiral center.

structure in the deprotonation of 2-butylcarbenium ion into 1-butene ($n_e = 3$) and 2-butene ($n_e = 1$). From data on the transformation of gas-phase carbenium ions from Dumesic et al.,[12] they calculated an elementary-step frequency factor for the deprotonation into 1-butene that was 3× larger than that for the deprotonation into 2-butene. This result strongly suggests that the intrinsic entropy change ($\Delta S°$) for (de)protonation elementary steps is independent of the structure.

The structure of the transition state is frequently unknown. Even though the estimation of the transition-state structure is possible by seeking the maximum-potential-energy structure along the reaction coordinate (minimum-energy pathway) in quantum-chemistry calculations, this powerful methodology becomes too costly in terms of the computational time when dealing with surface-bonded species and a large number of elementary steps. Therefore, shortcut formulas for the estimation of the number of single events, not requiring a detailed knowledge of the transition-state structure, were developed for hydride shift, methyl shift, PCP branching, β-scission, oligomerization, and hydride transfer.

The basic general structure of the transition state can be obtained from quantum-chemistry calculations. One of the key characteristics to be identified from transition-state structures is the retention of basic structural features of either the reactants (expected on exothermic elementary steps according to Hammond's postulate) or the products (expected on elementary steps where the intrinsic entropy change equals the entropy change upon reaction). In addition, identification of stretching bonds is also a key element to determine possible symmetry changes. Thus, formulas for the creation and/or destruction of symmetry axes and chiral centers yield a straightforward method for estimating the number of single events.

Table 2. Formulas for the Estimation of the Number of Single Events[a]

elementary step	formula	rationale
alkene protonation	$(n_e)_{prot} = 1$	transition state preserves the reactant structure: $\sigma^{\ddagger} = \sigma_r$
alkene deprotonation	$(n_e)_{deprot} = \sigma_{gl}(r)/\sigma_{gl}(p)$	alkene protonation reverse reaction
hydride shift	$(n_e)_{\beta s} = 2^{1+n1+n4}$	a 2-fold internal axis is created when 2 primary carbons are associated with the charge-bearing atom: $n1 = 1$ A 3-fold internal axis is created when 3 primary carbon atoms are attached to the carbon in β-position: $n4 = 1$
methyl shift	$(n_e)_{ms} = 2n_{\beta-Me\mid\ \alpha-carbon}$	transition state yields either 1 or 2 chiral centers depending on the number of methyl groups in β-position with respect to the α-carbon
PCP branching		a 2-fold internal axis is created when 2 primary carbon atoms are associated with the charge-bearing atom: $n1 = 1$
α-cleavage	$(n_e)_{pcp} = n_{\beta-H}\, 2^{1+n1+n2+n3}$	A chiral center is formed when 3 carbon atoms are attached to the carbon in α-position: $n2=1$
β-cleavage	$(n_e)_{pcp} = 2^{1+n1+n2+n3}$	A chiral center is formed when only 1 carbon atom is attached to the carbon in β-position: $n3 = 1$
oligomerization	$(n_e)_{olig} = [\sigma_{gl}(r_1)\sigma_{gl}(r_2)]/\sigma_{gl}(p)\ (n_e)_{\beta s}$	β-scission reverse reaction
β-scission	$(n_e)_{\beta s} = (2^{n1-n2-n3})/(3^{n4})$	2-fold internal axis is formed when 2 primary carbons are associated with the charged atom: $n1 = 1$ a chiral center is formed when 3 carbon atoms are attached to the carbon in α-position: $n2 = 1$ a chiral center is formed when only 1 carbon atom is attached to the carbon in β-position: $n3 = 1$ 3-fold internal axis is removed when 3 primary carbon atoms are attached to the carbon in β-position: $n4 = 1$
hydride transfer	$(n_e)_{ht} = [\sigma_{gl}(r_1)\sigma_{gl}(r_2)]/\sigma_{gl}^{\ddagger}$	transition state is set such that a 180° bond angle is formed between the two carbon centers: $\sigma^{\ddagger}$

[a] Letters (r) and (p) denote reactant and product, respectively. Double dagger indicates transition-state structures. By default, $n1 = n2 = n3 = n4 = 0$.

Table 2 shows a summary of the proposed short cut model formulas, together with the rationale behind them. Notice that, by taking advantage of the reversibility relationships, deprotonation and oligomerization formulas can be expressed in terms of the symmetry numbers of products and reactants. Molecular structures are, in general, readily available so that the estimation of their symmetry number is relatively easy.

Evans−Polanyi Relationship

Once the number of single events is available, a total of 8 frequency factors and 2836 energies of activation are left as kinetic parameters, assuming that all protonation equilibrium constants are known. In general, the energy of activation of each elementary step is strongly dependent on the nature and structure of the carbenium ions involved. Therefore, the impact of the carbenium-ion stability on the energy of activation is so significant that the exclusion of all steps leading to the formation of primary carbenium ions as transition states in the present model is based on such premises.

On the other hand, surface-bonded carbenium ions, which serve as stable intermediates, have a significantly weaker impact on the energy of activation. This is a consequence of the strong stabilization effect that the acid site delivers to the carbenium-ion structure by decreasing the energy of the surface-bonded ion to levels much closer to the levels of the species in the fluid phase. As the carbonyl bond stabilizes the carbenium ion by reducing its net charge, its associated surface-bonded ion retains most of the structural information, leading to a free carbenium ion as the transition state. Therefore, one of the minima along the reaction coordinate, either the reactant or the product, should resemble the structure of the transition state, whereas the other should not, thus establishing a correlation between the reactant−product energy difference and the energy of activation. This is the case for many elementary steps, as stated by the Evans−Polanyi relationship.[13]

The Evans−Polanyi relationship establishes that the magnitude of the energy barrier varies linearly with the energy change associated with the transformation. This functionality is expressed in terms of the energy of activation and the standard heat of reaction by means of eqs 20 and 21 for exothermic and endothermic elementary steps, respectively.

$$E_{aj} = E^{\circ}_{ElemStepType} - \alpha_{ElemStepType}|\Delta H_j^{\circ}| = E^{\circ}_{ElemStepType} + \alpha_{ElemStepType}\Delta H_j^{\circ}, \quad \Delta H_j^{\circ} < 0 \quad (20)$$

$$E_{aj} = E^{\circ}_{ElemStepType} + (1 - \alpha_{ElemStepType})|\Delta H_j^{\circ}| = E^{\circ}_{ElemStepType} + (1 - \alpha_{ElemStepType})\Delta H_j^{\circ}, \quad \Delta H_j^{\circ} > 0 \quad (21)$$

Here, an intrinsic energy barrier (E°), together with a transfer coefficient (α), enters into the energy of activation (E_{aj}) as a linearly dependent function of the standard heat of reaction (ΔH°). These expressions are consistent with TST, because the subtraction of the energies of activation for reversible elementary steps yields the correct magnitude and sign for the standard heat of reaction.

To account for energy differences between surface-bonded carbenium ions and their corresponding alkene isomers, Park and Froment[11] introduced the Evans−Polanyi relationship into the framework of the single-event kinetics. Because intrinsic energy barriers and transfer coefficients only depend on the type of elementary step, only 12 different parameters are required to set energy of activation values for all 2836 elementary steps. As a result, only three parameters per type of elementary step are required in order to calculate all the elementary-step rate coefficients, assuming that all the standard heats of reaction are available.

Stabilization Energies, Heats of Reaction, and Protonation Equilibrium Constants

So far, the proposed model requires only 18 independent kinetic parameters to calculate 2836 elementary-step rate

coefficients. The calculation of the rates of these steps also involves 78 protonation thermodynamics equilibrium constants and 2282 standard heats of reaction. Consequently, the energetics of the stabilization effect of a solid acid site on the energy of a surface-bonded carbenium ion must be considered. From the definition of the protonation equilibrium constant (K_p) (eq 5) in the protonation of the *i*th alkene to the *n*th ion, a more convenient expression is derived in which the Gibbs free energy change with protonation (ΔG_p) is split into different contributions:

$$K_p(R_i^=;R_n^+) = \exp\left(-\frac{\Delta G_p}{RT}\right) = \frac{\sigma_i}{\sigma_n}\exp\left(\frac{\Delta \hat{S}_p^\circ}{R} - \frac{\Delta H_p^\circ(R_i^=;R_n^+)}{RT}\right) \quad (22)$$

Equation 22 allows the calculation of protonation equilibrium constants as a function of the alkene-ion symmetry ratio, the intrinsic entropy change on protonation (ΔS_p°), and the heat of protonation at standard conditions (ΔH_p°). The derivation of eq 22 involves the application of the van't Hoff relationship, assuming that the heat of protonation at standard conditions for an alkene in the liquid phase is a weak function of temperature within the temperature range of interest (<390 K). When the intrinsic entropy change of protonation is assumed to be unique for all protonation elementary steps, only one additional parameter has to be determined from experimental data for a given catalyst.

The heat of protonation at standard conditions is defined as the algebraic sum of the enthalpies of formation for products and reactants:

$$\Delta H_p^\circ(R_i^=;R_n^+) = \Delta H_{f,s}^\circ(R_n^+) - \Delta H_{f,l}^\circ(R_i^=) - \Delta H_{f,s}^\circ(H^+) \quad (23)$$

In this expression, the enthalpies of formation for the surface-bonded species [$\Delta H_{f,s}^\circ(R_n^+)$ and $\Delta H_{f,s}^\circ(H^+)$] are unknown, whereas the enthalpy of formation of the alkene in the liquid phase [$\Delta HH_{f,l}^\circ(R_i^=)$] can be calculated from estimates for the alkene standard enthalpy of formation [$\Delta H_{f,g}^\circ(R_i^=)$] and the alkene standard heat of vaporization [$\Delta H_{vap}^\circ(R_i^=)$] by means of

$$\Delta H_{vap}^\circ(R_i^=) = \Delta H_{f,g}^\circ(R_i^=) - \Delta H_{f,l}^\circ(R_i^=) \quad (24)$$

To calculate the enthalpies of formation for surface-bonded species, the change in stabilization energy (Δq) is defined as the difference between the energy level of a free carbenium ion and that of its corresponding surface-bonded ion after stabilization on a solid acid site. Equation 25 relates Δq to the difference in the enthalpies of formation for the *n*th ion between the gas phase and the surface.

$$\Delta q(R_n^+) = \Delta H_{f,g}^\circ(R_n^+) - \Delta H_{f,s}^\circ(R_n^+) \quad (25)$$

For convenience, the stabilization energy (Δq_+) is defined as the difference between the stabilization energy change of the proton and that of the carbenium ion of interest. This definition establishes a convenient reference level for the stabilization energy at the energy level of the stabilized proton on a Brönsted acid site. This reference is specific for a given catalyst and circumvents setting the energy change of stabilization of the proton as a model parameter.

$$\Delta q_+(R_n^+) = \Delta q(H^+) - \Delta q(R_n^+) \quad (26)$$

The stabilization-energy definition allows the proper calculation of heats of protonation and standard heats of reaction. The calculation of heats of protonation and standard heats of reaction for the six elementary steps considered only requires the knowledge of the gas-phase enthalpies of formation and the carbenium-ion-dependent stabilization energies:

$$\Delta H_p^\circ(R_i^=;R_n^+) = \Delta H_{f,g}^\circ(R_n^+) - \Delta H_{f,g}^\circ(R_i^=) - \Delta H_{f,g}^\circ(H^+) + \Delta H_{vap}^\circ(R_i^=) + \Delta q_+(R_n^+) \quad (27)$$

$$\Delta H_j^\circ = \begin{cases} \text{pcp: } \Delta H_{f,s}^\circ(R_p^+) - \Delta H_{f,s}^\circ(R_r^+) = \Delta H_{f,g}^\circ(R_p^+) - \Delta H_{f,g}^\circ(R_r^+) \\ \text{hs: } \Delta H_{f,s}^\circ(R_p^+) - \Delta H_{f,s}^\circ(R_r^+) = \Delta H_{f,g}^\circ(R_p^+) - \Delta H_{f,g}^\circ(R_r^+) \\ \text{ms: } \Delta H_{f,s}^\circ(R_p^+) - \Delta H_{f,s}^\circ(R_r^+) = \Delta H_{f,g}^\circ(R_p^+) - \Delta H_{f,g}^\circ(R_r^+) \\ \beta\text{s: } \Delta H_{f,g}^\circ(R_p^+) - \Delta H_{f,g}^\circ(R_r^+) + \Delta q_+(R_p^+) - \Delta q_+(R_r^+) + \Delta H_{f,g}^\circ(R_p^=) \\ \text{olig: } \Delta H_{f,g}^\circ(R_p^+) - \Delta H_{f,g}^\circ(R_r^+) + \Delta q_+(R_p^+) - \Delta q_+(R_r^+) - \Delta H_{f,g}^\circ(R_r^=) \\ \text{ht: } \Delta H_{f,g}^\circ(R_p^+) - \Delta H_{f,g}^\circ(R_r^+) + \Delta q_+(R_p^+) - \Delta q_+(R_r^+) - \Delta H_{f,g}^\circ(R_r) + \Delta H_{f,g}^\circ(R_p) \end{cases} \quad (28)$$

The stabilization energy depends on both the nature of the acid site of the catalyst and the structure of the surface-bonded ion. When all the acid sites have the same strength, only one stabilization energy value per carbenium ion suffices to describe ion-surface interactions, so that the model contains 619 stabilization energies.

In the single-event kinetic modeling of the methanol-to-olefins process on ZSM-5 as well as on SAPO-34, Froment and coworkers[11,14] considered a common value for the stabilization energies of ions of the same carbon fraction. Application of a similar approach to the present model resulted in 10 stabilization energies, from $\Delta q_+(R^+_{C3})$ to $\Delta q_+(R^+_{C12})$. The large uncertainty on the parameter values, to be shown further, indicated that the available experimental data did not contain enough information. An inspection of the experimental results indeed reveals only a weak dependency on the temperature in the range of 353−393 K. Covering a broader temperature range by additional experiments below 330 K is unpractical because of too-low butene conversions, while experiments above 393 K are also unpractical by the liquid-phase condition, which is bounded by the isobutane critical temperature of 408 K.

The interaction of a carbenium ion with an acid site reduces its potential energy through the formation of a covalent carbonyl bond between a positively charged carbon atom and a negatively charged oxygen atom. The energy drop associated with the alkene protonation should strongly depend on both the acid strength of the active site and the molecular structure of the surface-bonded carbenium ion. Nevertheless, the present model assumes contributions to this drop in energy level for each acid site to be equal because of the unique acid strength among acid sites. In contrast, the dependency of the drop in energy level of surface-bonded ions does vary with structure in the gas phase. Hence, it is proposed that values for the energy of stabilization be expressed as a function of the variables that determine the energy level of a carbenium ion in the gas phase, i.e., the nature of the ion and its carbon number.

To establish a model for the catalyst-dependent stabilization energy as a function of the nature of the ion and the carbon number, two important contributions to stability have to be considered. There is a large contribution defined as the difference between the energy change on stabilization for a surface-bonded proton and a surface-bonded carbenium ion of a given ion-type (ΔE_+^{sec} or ΔE_+^{tert}). There is also a much smaller contribution (γ_c), accounting for the stabilization effect that an

Table 3. Isodesmic Reactions

	ion reactant	reactant molecule	product molecule	ion product	Δ
formula	CH_3CH_2+	CH_4	CH_3CH_3	CH_3+	
energy, Hartree/particle[a]	−78.525616	−40.316154	−79.464885	−39.311039	0.065846
energy, kcal/mol[b]	219.0	−17.9	−20.0	262.5	41.3
energy, kcal/mol (exp.)[b]				261.3	
formula	CH_3CH_2+	$CH_3CH_2CH_3$	CH_3CH_3	$CH_3CH_2CH_2+$	
energy, Hartree/particle[a]	−78.525616	−118.618098	−79.464885	−117.696194	−0.017365
energy, kcal/mol[b]	219.0	−25.0	−20.0	203.1	−10.9
energy, kcal/mol (Exp.)[b]				208.0	
formula	$(CH_3)_2CH+$	$(CH_3CH_2)_2CH_2$	$CH_3CH_2CH_3$	$(CH_3CH_2)_2CH+$	
energy, Hartree/particle[a]	−117.705733	−197.625783	−118.618098	−196.714381	−0.000963
energy, kcal/mol[b]	186.5	−35.1	−25.0	175.8	−0.6
energy,kcal/mol (exp.)[B]				173.0	

[a] Level of theory: PM2/6-31G++(d,p). [b] From ref 16.

increasing carbon number adds by distributing the positive charge along the carbon chain.

$$\Delta q_+(R_n^+) = \Delta E_+^{\text{sec}} + \gamma_c n_c(R_n^+) \quad (29)$$

$$\Delta q_+(R_n^+) = \Delta E_+^{\text{tert}} + \gamma_c n_c(R_n^+) \quad (30)$$

The application of eqs 29 and 30 is limited to a narrow range of carbon numbers. Assuming uniform neighboring stability effects, a linear decrease in stabilization energy with carbon number is expected for carbon-atom additions occurring relatively close to the charge-bearing carbon atom. In contrast, for carbon-chain growth occurring far from the charge-bearing carbon atom, stability effects become negligible, because of diminishing Coulomb interactions. A more-robust model for the stabilization energy would require a formulation based on a group contribution method, which would account for short-range interactions. Such a model would, however, require almost as many stabilization-related parameters as the one involving individual stabilization-energy values per carbon number.

The treatment proposed here and reflected in eqs 29 and 30 allows the reduction of the number of model parameters associated with the concept of stabilization energy from 619 to only 3. Adding these to the single intrinsic entropy change of protonation and to the 18 parameters associated with the kinetics of 6 different elementary steps, a total of 22 model parameters is obtained for the kinetic alkylation model.

Gas-Phase Enthalpies of Formation

Although data on gas-phase enthalpies of formation required for the calculation of heats of protonation and standard heats of reaction are available in the literature for molecular species such as alkanes and alkenes, they do not cover all the molecular species comprised in the reaction network. Consequently, the calculation of the standard enthalpy of formation for alkanes and alkenes in the gas phase is carried out by means of the group-contribution method formulated by Benson.[15] In principle, the Benson group-contribution method accounts for most of the atom-neighboring interactions within the molecule, assuming that these interactions are very short-ranged and that no strain energies exist along the molecule. Once the basic structure of an aliphatic hydrocarbon molecule is available, the application of the Benson group-contribution method is straightforward.

Energy Values for Carbenium Ions

The proposed model includes 619 carbenium ions acting either as intermediates (78) or deactivation agents (541). Their standard enthalpies of formation in the gas phase are required for the calculation of thermodynamic properties associated with protonation equilibria and energies of activation. Data on carbenium-ion energetics is scarce and, in most cases, inaccurate. Precise energy estimations can be obtained from quantum-chemical calculations, but the large number of species precludes such an approach. Again the Benson group-contribution method was adapted to account for the short-ranged interactions present within a carbenium ion. A judiciously selected set of data involving replicates for most of the seven additional ion-focused contributions that would be present in carbenium-ion structures is necessary to solve the resulting set of linear equations. By definition, the rank of the coefficient matrix associated with the linear set of equations is always lower than the number of Benson-like contributions, and therefore, the number of species (equations) used should be greater than the number of group contributions to permit the latter to be determined by multidimensional linear regression.

Because of the lack of sufficient data on carbenium-ion energetics, a combination of literature data and quantum-chemical calculations was used. Ab initio calculations were performed at the MP2/6-31G++(d,p) level of theory and brought to standard conditions by means of isodesmic reactions, i.e., reactions in which the total number of bonds and electrons are conserved.

The use of isodesmic reactions avoids error-prone calculations such as those required to take the quantum-chemical result for the ion energy at 0 K plus the zero-point energy to the enthalpy of a perfect gas at standard conditions. It also increases the accuracy of the estimation by canceling out electron-correlation effects which are often missed at moderate levels of theory. Table 3 illustrates the use of isodesmic reactions in the estimation of carbenium-ion standard enthalpies of formation.

Table 4 presents a data set comprising 19 different gas-phase carbenium ions used in the Benson contributions estimation. In this set, four primary carbenium ions are included to bring consistency into the Benson-like structure. The method turned out to be remarkably accurate, with a sample standard error of ~8.1 kJ/mol.

Figure 1 is a parity plot comparing Benson-like estimates with values for the standard energies of formation of carbenium ions from Table 4. As expected, the most influential element determining the energy level of a free carbenium ion is its nature, but the data also reveal an important overlap among the energies of some secondary and tertiary ions due to the impact of the carbon number on their relative stability.

In what follows, thermodynamic constraints are applied to achieve further reductions in the number of model parameters as well as in the number of species required to characterize the

Table 4. Gas-Phase Carbenium-Ion Standard Enthalpy of Formation[a]

		gc												
carbenium ion	group	1	2	3	4	12	13	14	15	16	17	18	ΔHf° kJ/mol (exp)[b]	ΔHf° kJ/mol (calc)
ethyl	O2[p]	0	0	0	0	1	0	0	1	0	0	0	917	901
n-propyl	O3[p]	1	0	0	0	1	0	0	0	1	0	0	871	871
n-butyl	O4[p]	1	1	0	0	1	0	0	0	1	0	0	842	851
n-pentyl	O5[p]	1	2	0	0	1	0	0	0	1	0	0	833	830
s-propyl	O3[s]	0	0	0	0	0	1	0	2	0	0	0	781	777
s-butyl	O4[s]	1	0	0	0	0	1	0	1	1	0	0	747	748
s-pentyl(2)	O5[s]	2	0	0	0	0	1	0	0	2	0	0	724[c]	718
s-hexyl(2)	O6[s]	1	2	0	0	0	1	0	1	1	0	0	712	706
s-heptyl(2)	O7[s]	1	3	0	0	0	1	0	1	1	0	0	678	686
2,4-dimethylpentyl(3)	DO7[s]	4	0	0	0	0	1	0	0	0	2	0	649[c]	634
2,2,4,4-tetramethylpentyl(3)	QO9[s]	6	0	0	0	0	1	0	0	0	0	2	596[c]	572
tert-butyl	MO4[t]	0	0	0	0	0	0	1	3	0	0	0	687	680
2-methylbutyl(2)	MO5[t]	1	0	0	0	0	0	1	2	1	0	0	654	650
2-methylpentyl(2)	MO6[t]	1	1	0	0	0	0	1	2	1	0	0	631	630
3-methylpentyl(3)	MO6[t]	2	0	0	0	0	0	1	1	2	0	0	629	621
2,3-dimethylbutyl(2)	DO6[t]	2	0	0	0	0	0	1	2	0	1	0	620	608
2-methylhexyl(2)	MO7[t]	1	2	0	0	0	0	1	2	1	0	0	619	609
2,4-dimethylpentyl(2)	DO7[t]	2	0	1	0	0	0	1	2	1	0	0	609	600
2,3,3-trimethylbutyl(3)	TO7[t]	3	0	0	0	0	0	1	2	0	0	1	593	577

[a] ΔHf° values from Benson-like method with gc1[C − CH3] = −42.19, gc2[C − C2H2] = −20.64, gc3[C − C3H] = −7.95, gc4[C − C4] = 2.09, gc12[C + (−CH2)] = 942.8, gc13[C + (−C2H)] = 861.2, gc14[C + (−C3)] = 806.3, gc15[C − C + H3] = −42.18, gc16[C − C + CH2] = −29.33, gc17[C − C + C2H] = −29.41, gc18[C − C + C3] = −18.03 in kJ/mol. [b] From ref 17. [c] Level of theory: PM2/6-31G++(d,p).

reaction mixture without losing detail at the elementary-step level description.

Thermodynamic Constraints and Lumping of Components

By looking at the reaction-product composition, there is some indication that species sharing the same degree of branching within a given carbon fraction might be very close to equilibrium. For instance, partition coefficients for butene isomers, extracted from experimental data at 393 K, turned out to be in good agreement with calculated values for equilibrium conditions, as shown in Table 5. In this table, a 1-butene/2-butene partition coefficient obtained from Gibbs free energy minimization is compared with values drawn from experiments at various process-times for a given total butene space-time.

Assuming nonbranching isomerization rates for aliphatic hydrocarbons increase with carbon number infers that equilibrium conditions prevail for all species with a carbon number >4. This implies that the reaction rates for nonbranching isomerization elementary steps, such as hydride shift and methyl shift, achieve equilibrium at reaction conditions. Consequently, rates corresponding to 65 hydride shifts and 29 methyl shifts can now be replaced by equilibrium relationships. The number of model parameters is reduced from 22 to 16, while the number of rates of elementary steps to be calculated becomes 2742.

Additionally, at a given temperature, nonbranching isomerization equilibrium fixes the composition within a component group or "lump" consisting of alkenes with similar carbon number and degree of branching and eliminates the need for rate coefficients for these steps. When 13 such lumps are considered for alkenes (O3, O4, MO4, MO5, DO5, MO6, DO6, MO7, DO7, TO7, MO8, DO8, and TO8), the number of components in the liquid phase (v-responses) is reduced from 134 (103 alkenes + 31 alkanes) to 44 (13 alkene lumps + 31 alkanes).

If the nonbranching steps reach equilibrium, the mole fraction, $[x(R_k^=)]$, of any member of the lump of alkenes may be written in terms of the liquid-phase Gibbs free energies of formation, $(\Delta G_{f,l})$:

$$x^{cg}(R_r^=) = \sum_{k=1}^{N} x(R_k^=) = x(R_r^=)\left[1 + \sum_{k\neq r}^{N-1}\left(\frac{\Delta G_{f,l}(R_k^=) - \Delta G_{f,l}(R_r^=)}{RT}\right)\right] = x(R_r^=)\mathrm{LC}(R_r^=) \quad (31)$$

Equation 31 also introduces lumping coefficients $\mathrm{LC}(R_r)$. The lumping coefficient is a thermodynamic quantity that solely depends on temperature. It is expressed in eq 32, after canceling out all nonstructural contributions to the entropy, as a function of the enthalpies of formation in the liquid phase, $(\Delta H_{f,l})$.

$$\mathrm{LC}(R_r^=) = 1 + \sum_{k\neq r}^{N-1}((\sigma_{gl}(R_r^=)/\sigma_{gl}(R_k^=)))(-(\Delta Hf_{f,l}(R_k^=) - \Delta H_{f,l}(R_r^=)/RT)) \quad (32)$$

The enthalpies of formation in the liquid phase are calculated from eq 33, given the standard enthalpy of formation $(\Delta H_{f,g}^\circ)$ and neglecting the enthalpy dependency on pressure. The second term is the enthalpy change of vaporization (ΔH_{vap}°) at standard conditions. Finally, the temperature of interest is reached by an isobaric enthalpy change, involving the liquid heat capacity (C_{liq}).

$$\Delta H_{f,l}(R_k^=) = \Delta H_{f,g}^\circ(R_k^=) - \Delta H_{vap}^\circ(R_k^=) + \int_{T^\circ}^{T} C_{liq}(R_k^=)\,dT \quad (33)$$

Liquid heat capacities and enthalpy changes by vaporization for the 134 species in the liquid phase were calculated from

two group-contribution methods taken from the literature. The method of Rùzicka and Domalski[18] was applied to the estimation of the liquid heat capacity of aliphatic hydrocarbons as a function of temperature in the range between the melting temperature and the normal boiling temperature. It is based on a set of structural contribution parameters adjusted by means of liquid heat capacity data for >1300 organic liquids. The contributions include atom-neighboring interactions within the molecule.

A group-contribution method developed by Constantinou and Gani[19] was used in the estimation of the enthalpy change by vaporization at standard conditions. In general, this method does not consider atom-neighboring interactions. Once individual group contributions within the molecule have been identified, they are used to obtain estimates for the value of the enthalpy change by vaporization.

Another thermodynamic constraint leading to a further reduction in the number of model parameters is derived from the reversibility condition relating oligomerization and β-scission elementary steps. TST then establishes that common values for the intrinsic energy barrier ($E°$) and the transfer coefficient (α) must be applied to both elementary steps, since the subtraction of the energies of activation for reversible elementary steps must yield the standard heat of reaction. The β-scission single-event frequency factor then ends up as the only independent model parameter necessary to determine the rates of 554 β-scission elementary steps.

In conclusion, thermodynamic constraints comprising the rigorous lumping of species in equilibrium and the reversibility of oligomerization/β-scission elementary steps enable the formulation of a realistic kinetic model at the elementary-step level for the solid acid alkylation of isobutane with butenes comprising only 14 model parameters to describe the kinetics of 2742 elementary steps between 753 species.

Rate Expressions at the Single-Event Level

So far a consistent methodology has been applied to the elementary-step level description of the kinetics of solid acid alkylation, aiming for a more tractable model based on the single-event kinetics. The rates at the elementary-step level can be expressed in terms of the rates at the single-event level, in which 14 model parameters, 44 molar fractions for lumps in the liquid bulk, and 541 surface concentrations of irreversibly adsorbed species are needed for a complete kinetic description. Equation 34 summarizes the most relevant features of a 2742-dimensional reaction rate vector ($\mathbf{r}_j$), which comprises the single-event rate coefficients.

$$\mathbf{r}_j = \begin{cases} n_{e_j}\tilde{A}_{\mathrm{pcp}} \exp\left(-\dfrac{E°_{\mathrm{pcp}} + \alpha_{\mathrm{pcp}}\Delta H°_j}{RT}\right) K_{\mathrm{p}}(R_i^{=};R_n^{+}) \left(\dfrac{V_{\mathrm{L}}}{V_{\mathrm{p}}}\right) \bar{C}_{\mathrm{sat}} C^{\mathrm{t}}_{\mathrm{H}^+} \left(\dfrac{\varphi}{1+\theta_{\mathrm{rev}}}\right) \dfrac{x^{\mathrm{cg}}(R_i^{=})}{\mathrm{LC}(R_i^{=})} \\ n_{e_j}\tilde{A}_{\beta\mathrm{s}} \exp\left(-\dfrac{E°_{\mathrm{olig}} + (1-\alpha_{\mathrm{olig}})\Delta H°_j}{RT}\right) K_{\mathrm{p}}(R_i^{=};R_n^{+}) \left(\dfrac{V_{\mathrm{L}}}{V_{\mathrm{p}}}\right) \bar{C}_{\mathrm{sat}} C^{\mathrm{t}}_{\mathrm{H}^+} \left(\dfrac{\varphi}{1+\theta_{\mathrm{rev}}}\right) \dfrac{x^{\mathrm{cg}}(R_i^{=})}{\mathrm{LC}(R_i^{=})} \\ n_{e_j}\tilde{A}_{\mathrm{olig}} \exp\left(-\dfrac{E°_{\mathrm{olig}} + \alpha_{\mathrm{olig}}\Delta H°_j}{RT}\right) K_{\mathrm{p}}(R_i^{=};R_n^{+}) \left(\dfrac{V_{\mathrm{L}}}{V_{\mathrm{p}}}\right) \bar{C}^2_{\mathrm{sat}} C^{\mathrm{t}}_{\mathrm{H}^+} \left(\dfrac{\varphi}{1+\theta_{\mathrm{rev}}}\right) \dfrac{x^{\mathrm{cg}}(R_i^{=})}{\mathrm{LC}(R_i^{=})} \dfrac{x^{\mathrm{cg}}(R^{=})}{\mathrm{LC}(R^{=})} \\ n_{e_j}\tilde{A}_{\mathrm{ht}} \exp\left(-\dfrac{E°_{\mathrm{ht}} + \alpha_{\mathrm{ht}}\Delta H°_j}{RT}\right) K_{\mathrm{p}}(R_i^{=};R_n^{+}) \left(\dfrac{V_{\mathrm{L}}}{V_{\mathrm{p}}}\right) \bar{C}^2_{\mathrm{sat}} C^{\mathrm{t}}_{\mathrm{H}^+} \left(\dfrac{\varphi}{1+\theta_{\mathrm{rev}}}\right) \dfrac{x^{\mathrm{cg}}(R_i^{=})}{\mathrm{LC}(R_i^{=})} x(R) \\ n_{e_j}\tilde{A}_{\beta\mathrm{s}} \exp\left(-\dfrac{E°_{\mathrm{olig}} + (1-\alpha_{\mathrm{olig}})\Delta H°_j}{RT}\right) C_{R_{\mathrm{m}}^+} \end{cases} \tag{34}$$

with

$$\theta_{\mathrm{rev}} = \sum_{n=1}^{N} K_{\mathrm{p}}(R_i^{=};R_n^{+}) \left(\frac{V_{\mathrm{L}}}{V_{\mathrm{p}}}\right) \bar{C}_{\mathrm{sat}} \frac{x^{\mathrm{cg}}(R_i^{=})}{\mathrm{LC}(R_i^{=})} \tag{35}$$

Equation 35 is the final expression for the reversible fractional site coverage (θ_{rev}) as a function of the composition of the liquid bulk, expressed in terms of the molar fractions.

Reactor Model

To obtain the independent parameters from the experimental data, the set of eqs 34 and 35 has to be inserted into a model for the fixed-bed isothermal reactor used in this work. The reactor-geometry and operating conditions, such as the superficial flow velocity together with the catalyst particle size, justify a pseudo-homogeneous, one-dimensional model with plug flow for the reactor (eq 36) that describes the evolution of the vector of product yields (Y) with butene space-time ($\mathrm{W/F°_{O4}}$) and contains the stoichiometric coefficient matrix (ν^{f}) for the liquid phase, the diagonal matrix of molecular weights (**M**), and the vector of reaction rates. The product of the 44 × 2742 stoichiometric coefficient matrix, which provides relationships derived from the reaction network, with the 2742-dimensional vector of reaction rates delivers a 44-dimensional vector with the net production rates for each component of the liquid phase.

$$\frac{\partial \hat{Y}}{\partial(\mathrm{W/F°_{O4}})} = \frac{(3600)100 M_{\mathrm{O4}}}{1 + F°_{\mathrm{MP4}} M_{\mathrm{MP4}}/F°_{\mathrm{O4}} M_{\mathrm{O4}}} \mathbf{M}\nu^{\mathrm{f}}\bar{r}(\hat{Y},\bar{C}_{\mathrm{R}_{m^+}}) \tag{36}$$

$$\hat{Y} = \{\hat{Y}_1, \hat{Y}_2, ..., \hat{Y}_{\mathrm{v}}\}^{\mathrm{T}} \tag{37}$$

As a consequence of catalyst deactivation, the reactor operates in the transient state. The product yield profiles along the reactor vary as the number of irreversibly covered sites increases with process-time. These changes are accounted for in eq 36 through the reaction-rate dependency on the surface concentrations of the irreversibly adsorbed ions ($C_{\mathrm{R}m+}$). Accumulation of these species in the solid phase is responsible for the catalyst deactivation and dictates the evolution of the profiles with process-time. Equation 36 does not contain a time derivative, because the accumulation of matter in the liquid phase is negligible. Even though there is a significant change in the number of moles of alkene species in the reaction mixture, the accumulation term is neglected because the overall concentration remains almost constant because of its high dilution in isobutane.

Table 5. Non-Branching Isomerization Equilibrium Test[a]

species	equilibrium composition[c] @ 393 K	experimental composition[b] @ 393 K: butene space-time[d] 0.4	butene space-time[d] 0.7	butene space-time[d] 1.0
1-butene	0.091	0.091	0.105	0.096
2-butene (*z*−/*e*−)	0.909	0.909	0.895	0.904
2-butene/1-butene partition coefficient	10.0	10.0	8.5	9.5

[a] Alkenes within the O4 component group. [b] Experimental values at process-time 1.17, 0.50, and 0.40 h. [c] From Gibbs free energy minimization. [d] Butene space-time units are h·gCat/mol.

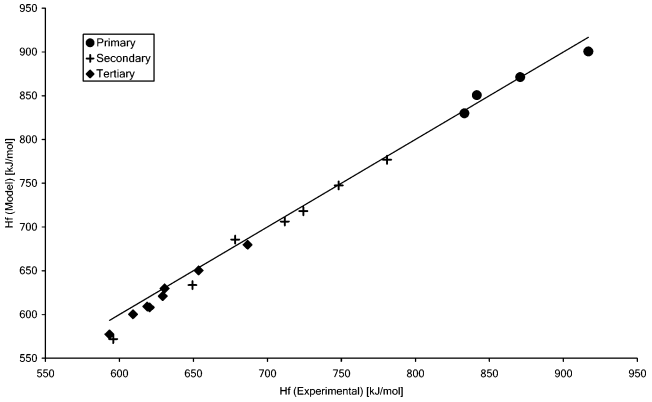

Figure 1. Standard enthalpy of formation of carbenium ions, parity plot.

As mentioned before, irreversibly adsorbed species can undergo surface elementary steps, such as hydride shift, methyl shift, and PCP branching, which can be assumed to be quasi-equilibrated because of the irreversibilily of their adsorption. Surface elementary steps involving desorption of a C_9+ ion, such as hydride transfer and deprotonation, are explicitly forbidden. Oligomerization and β-scission steps are limited to those required for the formation of the C_9+ ion and the corresponding reverse steps.

To account for the irreversibly adsorbed species in the model, conservation principles are applied to the solid surface, so that the accumulation of these species can be written in terms of the reaction rates. In eq 38, the evolution with process-time of the vector of surface concentrations for the irreversibly adsorbed ions is a function of the stoichiometric coefficient matrix for the solid phase (ν^s) and the vector of reaction rates. Here, the 541×2742 stoichiometric coefficient matrix comprises all the reaction network relationships involving irreversibly adsorbed ions.

$$(\partial/\partial t)\bar{C}_{\mathrm{R}_m^+} = (3600)\nu^s \bar{r}(\hat{Y}, \bar{C}_{\mathrm{R}_m^+}) \tag{38}$$

$$\bar{C}_{\mathrm{R}_m^+} = \{\bar{C}_{\mathrm{R}_1^+}, \bar{C}_{\mathrm{R}_2^+}, ..., \bar{C}_{\mathrm{R}_M^+}\}^{\mathrm{T}} \tag{39}$$

Equations 38 and 39 form a set of partial differential equations (PDEs) describing the evolution of the liquid-phase molar flow rates and the surface concentration of irreversible adsorbed ions with butene space-time and process-time. The structure of the PDE suggests an integration strategy based on the discretization of both process-time and butene space-time. Consequently, the discretization process leads to the separation of the PDE problem into a set of nonlinear first-order ordinary differential equations (ODEs) described by eq 36 and a set of linear first-order ODEs with constant coefficients represented by eq 40.

$$C_{\mathrm{H}+}^{\mathrm{t}}\left(\frac{\partial}{\partial t}\right)\left(\frac{C_{\mathrm{R}_m^+}}{C_{\mathrm{H}+}^{\mathrm{t}}}\right) = (\sum_{j=1} r'_{j,\mathrm{olig}})\left(1 - \sum_{k=1}^{M}\frac{C_{\mathrm{R}_k^+}}{C_{\mathrm{H}+}^{\mathrm{t}}}\right) - (\sum_{j=1} r'_{j,\beta\mathrm{s}})\left(\frac{C_{\mathrm{R}_m^+}}{C_{\mathrm{H}+}^{\mathrm{t}}}\right) \tag{40}$$

The integration strategy yields two coupled initial value problems (IVPs). In the first IVP, a 44-dimensional ODE set described by eq 36 is integrated for a given process-time along the butene space-time by means of the numerical differentiation formula (NDF) scheme for stiff problems implemented by Shampine and Reichelt.[20] The initial conditions are the inlet yields:

$$\hat{Y}(\mathrm{W/F}_{\mathrm{O4}}^{\circ}\, M_{\mathrm{O4}} = 0, t) = \hat{Y}^{\circ} \tag{41}$$

The second set, a 541-dimensional eigenvalue problem described by eq 40, has an analytical solution based on the diagonalization of the constant coefficient matrix. Because a fresh load of catalyst was used for each experimental run, the initial condition for the solution of this set for a given butene space-time is given by

$$\bar{C}_{\mathrm{R}_m^+}(\mathrm{W/F}_{\mathrm{O4}}^{\circ}\, M_{\mathrm{O4}}, t = 0) = 0 \tag{42}$$

Steps in butane space-time and process-time are sequentially halved until differences between two consecutive solution grids become negligible.

Asymptotic solutions provide interesting insights into the fixed-bed operation of this process. In the first place, when the butene space-time tends to infinity, the concentration of limiting reactants tends to zero and the reversible reactions reach equilibrium. In the mathematical model, this is equivalent to neglecting the derivative with respect to butene space-time, so that eq 36 turns into eq 43. At equilibrium, the product yields at the reactor exit no longer depend on the butene space-time, so that a flat profile is observed for a given level of deactivation, i.e., a given profile of irreversibly adsorbed ions.

$$\nu^{\mathrm{f}} \bar{r}(\hat{Y}^{\mathrm{eq}}, \bar{C}_{\mathrm{R}_m^+}) = 0 \tag{43}$$

When the process-time tends toward infinity, steady state operation is achieved and both the product yield and the surface concentration of the irreversibly adsorbed ions become independent of process-time.

$$\nu^s\, \bar{r}(\hat{Y}, \bar{C}_{\mathrm{R}_m^+}^{\infty}) = 0 \tag{44}$$

Table 6. Constraints on Parameters

Parameter(s)	Linear Constraint	Rationale
$\frac{E^{\circ}_{pcp}}{R\alpha_{pcp}}, \frac{E^{\circ}_{olig}}{R\alpha_{olig}}, \frac{E^{\circ}_{ht}}{R\alpha_{ht}}$	$\frac{Ea_j}{R} = \frac{E^{\circ}_{ElemStepType}}{\alpha_{ElemStepType}R} + \frac{\Delta H^{\circ}_j}{R}, \Delta H^{\circ}_j < 0$	Energy of activation must be a positive quantity
$\alpha_{pcp}, \alpha_{olig}, \alpha_{ht}$	$0 < \alpha_{ElemStepType} < 1$	Energy of activation must be a fraction of the intrinsic energy barrier
$\frac{\Delta E^{sec}_{+}}{R}, \frac{\Delta E^{tert}_{+}}{R}, \frac{\gamma_c}{R}$	$-200\ \frac{kJ}{mol} < \frac{\Delta H^{\circ}_p\left(R^{=}_i; R^{+}_n\right)}{R} < 0$	Heat of Protonation must be exothermic with a lower bound of about -200 kJ/mol.
$\frac{\Delta E^{sec}_{+}}{R}, \frac{\Delta E^{tert}_{+}}{R}, \frac{\gamma_c}{R}$	$\frac{\Delta H^{\circ}_p\left(R^{=}_x; R^{+}_{nx}\right)}{R} < \frac{\Delta H^{\circ}_p\left(R^{=}_y; R^{+}_{ny}\right)}{R}, n_C(R^{=}_x) > n_C(R^{=}_y)$	For similar types of carbenium ions, the magnitude of the heat of protonation must increase with the carbon number
$\frac{\Delta \hat{S}_p}{R}$	$\frac{\Delta \hat{S}_p}{R} < 0$	Intrinsic entropy must decrease on protonation
$\frac{\Delta E^{sec}_{+}}{R}$	$\frac{\Delta E^{sec}_{+}}{R} > 0$	Stabilization energy of a secondary carbenium ion must be positive
$\frac{\Delta E^{tert}_{+}}{R}$	$\frac{\Delta E^{tert}_{+}}{R} > 0$	Stabilization energy of a tertiary carbenium ion must be positive
$\frac{\gamma_c}{R}$	$\frac{\gamma_c}{R} < 0$	Stabilization energy should decrease with carbon number

In all the experimental runs, the operation reached steady state with respect to process-time. An even more relevant observation is that the conversion has not dropped to zero when the steady state was reached. This observation strongly supports the approach taken in the present reactor model concerning the reactivity of the irreversibly adsorbed ions.

A complete solution of the present reactor model for a typical process-time of ~8 h in a 100 × 100 grid consumes a significant amount of computational time. To complete the parameter estimation process in a realistic amount of time, the computer program switches to the corresponding asymptotic solution when the integration code identifies the occurrence of equilibrium or steady-state conditions

Parameter Estimation

The parameter estimation was based on the treatment presented in Froment and Bischoff[21] and also involves statistical tests.

The model equation is represented by

$$\hat{Y}_h = f_h(\bar{X}_i, \bar{\beta}), \quad h = 1, ..., v \tag{45}$$

where $\bar{\beta}$ is the parameter vector

$$\bar{\beta} = \{\tilde{A}_{pcp}, E^{\circ}_{pcp}, \alpha_{pcp}, \tilde{A}_{olig}, E^{\circ}_{olig}, \alpha_{olig}, \tilde{A}_{ht}, E^{\circ}_{ht}, \alpha_{ht}, \tilde{A}_{\beta s}, \Delta\hat{S}_p, \Delta E^{sec}_{+}, \Delta E^{tert}_{+}, \gamma_c\} \tag{46}$$

The multiresponse objective function is written

$$S(\bar{\beta}) = \sum_{h=1}^{v}\sum_{k=1}^{v}\omega_{h,k}\sum_{i=1}^{n}[Y_{i,h} - f_h(\bar{X}_i, \bar{\beta})][Y_{i,k} - f_k(\bar{X}_i, \bar{\beta})] \tag{47}$$

The evaluation of the objective function (eq 47) for a given set of parameters involves the 79 experiments (n) with each of the 44 responses (v) of the 9 runs.

Constrained-parameter estimation was performed to account for the physicochemical constraints imposed by the fundamental nature of the parameters of the model. By alternating the use of two algorithms for constrained and unconstrained optimization, the parameters were iteratively improved. For constrained optimization, a sequential quadratic programming (SQP) algorithm was used, together with the parameter constraints presented in Table 6. In general, the solution of a constrained optimization problem involves the solution of several quadratic programming (QP) subproblems by means of an unconstrained optimization algorithm. For problems that are nonlinear in the parameters, such as the present one, the formulation of the QP subproblem involves not only the linearization of the objective function but also the inclusion of linear constraints. Details about the SQP algorithm and its implementation are reported by Grace.[22] Once the constrained optimization procedure is terminated, the solution from this algorithm is fed to an implementation of the Marquardt algorithm to ensure that the solution corresponds to a minimum where the gradient of the multiresponse objective function is zero. This zero-gradient condition must be satisfied to properly apply statistical tests on the significance of the parameters. The model parameters of eq 46 were reparametrized into those shown in eq 48.

$$\bar{\beta} = \left\{\ln \tilde{A}_{pcp}, \frac{E^{\circ}_{pcp}}{R\alpha_{pcp}}, \alpha_{pcp}, \ln \tilde{A}_{olig}, \frac{E^{\circ}_{olig}}{R\alpha_{olig}}, \alpha_{olig}, \ln \tilde{A}_{ht}, \frac{E^{\circ}_{ht}}{R\alpha_{ht}}, \alpha_{ht}, \ln \tilde{A}_{\beta s}, \frac{\Delta\hat{S}_p}{R}, \frac{\Delta E^{sec}_{+}}{R}, \frac{\Delta E^{tert}_{+}}{R}, \frac{\gamma_c}{R}\right\} \tag{48}$$

Instead of the single-event frequency factors the normal logarithms are estimated. This ensures positive values for these parameters and improves convergence by making changes on these large numbers more significant. Intrinsic energy barriers were reparametrized by dividing them by the transfer coefficients. These ratios reduce the correlation between the two parameters and facilitate the formulation of linear constraints on them. Energy-related parameters are divided by the universal gas constant (R) to scale them and to simplify the management of engineering units. The reparametrized vector shown in eq 48 is used in both the constrained and unconstrained optimizations. The parameter constraints shown in Table 6 are derived from the fundamentals of the TST and thermodynamics. In most cases, their rationale, as well as their implementation, is obvious. In addition, some constraints involve linear combinations of several parameters in one expression. Full application to the model yields 2118 linear constraints.

The formulation of statistical tests for models and parameters in nonlinear regression methods followed the treatment described

Table 7. Parameter Estimates

parameters[a]	estimates	95% approx. conf. interval	$\|t$ − value $\|$[b]	parameters	values	units
$\ln \tilde{A}_{pcp}$	2.901×10^{1}	$\pm 4.46 \times 10^{1}$	4.03	$\tilde{A}_{pcp}$	3.97×10^{12}	s^{-1}
$(E^{\circ}_{pcp}/R\alpha_{pcp})$	1.433×10^{4}	$\pm 1.88 \times 10^{2}$	4.77	E°_{pcp}	7.15×10^{1}	kJ/mol
α_{pcp}	6.001×10^{-1}	5.30×10^{-3}	7.02	α_{pcp}	6.00×10^{-1}	dimensionless
$\ln \tilde{A}_{olig}$	1.794×10^{1}	$\pm 5.20 \times 10^{-2}$	21.39	$\tilde{A}_{olig}$	6.18×10^{7}	s^{-1}·gCat/mol
$(E^{\circ}_{olig}/R\alpha_{olig})$	1.518×10^{4}	$\pm 1.51 \times 10^{1}$	62.46	E°_{olig}	7.59×10^{1}	kJ/mol
α_{olig}	6.015×10^{-1}	$\pm 2.04 \times 10^{3}$	18.23	α_{olig}	6.02×10^{-1}	dimensionless
$\ln \tilde{A}_{ht}$	3.523×10^{1}	$\pm 1.13 \times 10^{1}$	19.39	$\tilde{A}_{ht}$	1.99×10^{15}	s^{-1}·gCat/mol
$(EE^{\circ}_{ht}/R\alpha_{ht})$	1.262×10^{5}	$\pm 1.33 \times 10^{2}$	58.76	E°_{ht}	9.18×10^{1}	kJ/mol
α_{ht}	8.749×10^{-2}	$\pm 2.01 \times 10^{-4}$	26.93	α_{ht}	8.70×10^{-2}	dimensionless
$\ln \tilde{A}_{\beta s}$	1.382×10^{1}	$\pm 1.30 \times 10^{-2}$	66.09	$\tilde{A}_{\beta s}$	2.04×10^{6}	s^{-1}
$(\Delta \hat{S}_p/R)$	-2.177×10^{1}	$\pm 2.96 \times 10^{-2}$	45.64	ΔS_p	-1.81×10^{2}	J/(mol·K)
$(\Delta E^{sec}_{+}/R)$	8.648×10^{4}	$\pm 4.25 \times 10^{1}$	126.04	ΔE^{sec}_{+}	7.19×10^{2}	kJ/mol
$(\Delta E^{tert}_{+}/R)$	9.141×10^{4}	$\pm 3.33 \times 10^{1}$	170.02	ΔE^{tert}_{+}	7.60×10^{2}	kJ/mol
(γ_c/R)	3.019×10^{2}	$\pm 4.82 \times 10^{3}$	0.0039	γ_c	2.51×10^{0}	kJ/mol

[a] After reparametrization. Significance of regression (F-test) yields an F-value of 2589 to reject the lack-of-fit hypothesis with F critical value of 0.70. [b] Estimates significantly different from zero for values greater than the t critical value of 2.24

by Gallant.[23] This treatment allows the formulation of statistics in nonlinear regression by means of model linearization.

Results and Discussion

Because of the large amount of computing time required to evaluate the objective function, not all 79 available data sets were used in the parameter estimation. 26 data sets pertaining to the steady state were left out.

The parameter confidence intervals shown in Table 7 indicate that, for most of the parameters, reasonably accurate and significant estimates are determined. The estimates of the PCP parameters have broader confidence intervals and appear to be less accurate.

The estimate for the carbon-number contribution to the stabilization energy is not significantly different from zero at the 95% confidence level, suggesting that the stabilization-energy dependency on the nature of the carbenium ion has a greater importance than its dependency on the carbon number, at least for proton-exchanged Y-zeolites at moderate temperatures. On the other hand, this trend could also be a consequence of the weak temperature dependence observed in the experimental data.

In general, the values of the estimated parameters are in reasonable agreement with those reported elsewhere, but the value of 0.6 obtained for the Evans−Polanyi transfer coefficient for oligomerization contradicts the general expectancy that values of the transfer coefficient for highly exothermic elementary steps such as oligomerization should be <0.5. In the kinetic modeling of the methanol-to-olefins (MTO) process over ZSM-5 and SAPO-34. Froment et al.[2,14] obtained estimates significantly <0.5.

Parity plots for the most relevant product yields are presented in Figures 2−5. The model is very successful for the prediction of the major reaction products O4, [M+D+T]P8, and [M+D+T]-O8 and evidently less successful with minor products such as P5, P6, and P7. Also, the model underestimates the values for [M+D+T]O8 and P5−P7, whereas it slightly overestimates [M+D+T]P8 values.

Figure 6 shows the evolution with process-time of model-predicted and experimental reactor-exit yields for the most-significant component groups. The calculated trends reproduce the most relevant features of the experimental fixed-bed behavior. The oligomerization is fast and so is the deactivation. Because of this, it is located in a narrow zone moving through the bed and is hardly observed at the exit until breakthrough of the deactivation zone. The yield of C_8 paraffins then sharply

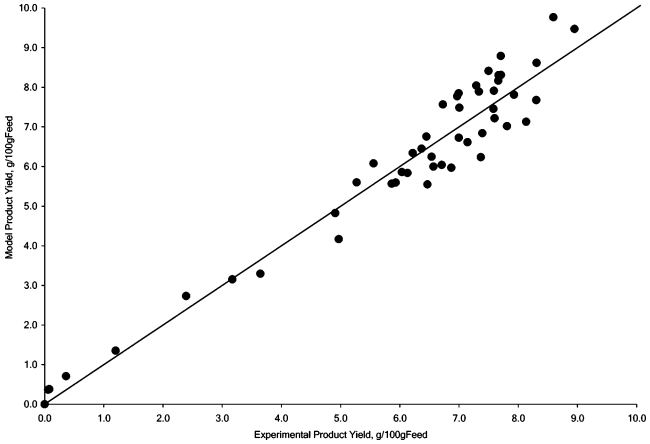

Figure 2. Parity plot for O4 product yield.

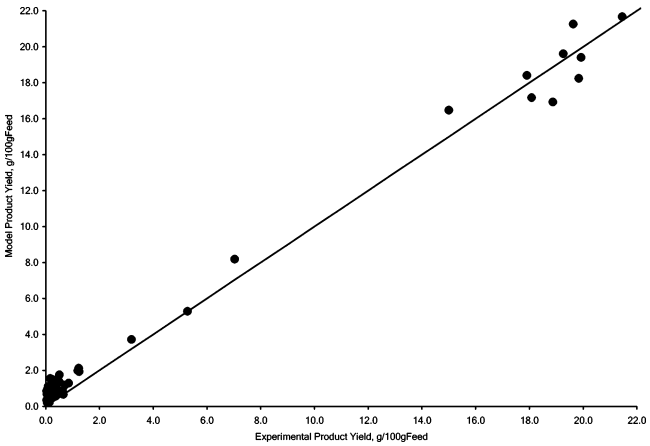

Figure 3. Parity plot for [M+D+T]P8 product yield.

drops, but not to zero. A strong selectivity shift from saturated to unsaturated products is observed.

The simulation strongly supports the proposed deactivation mechanism based on an irreversible site coverage by oligomers which retain a certain reactivity. Dibranched octenes are subject to β-scission, and this leads to a dynamic equilibrium concentration of deactivating species on the catalyst. It also corroborates the hypothesis that hydride-transfer steps, which could help avoid deactivation, actually deactivate faster than any other elementary step, because of their dependency on the availability of neighboring acid sites. Figure 6 shows how the model leads to a nonzero conversion steady state. This confirms that

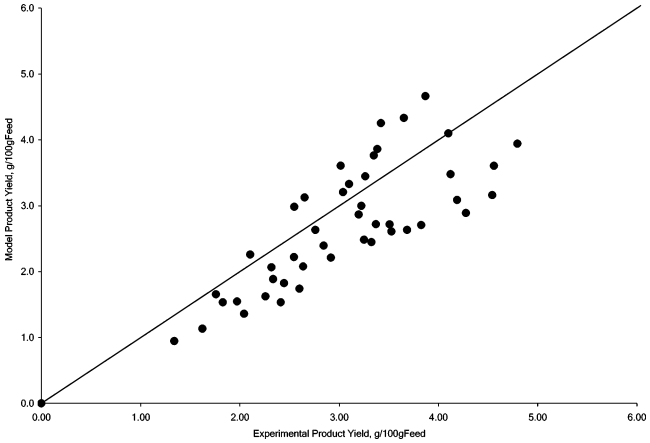

Figure 4. Parity plot for [M+D+T]O8 product yield.

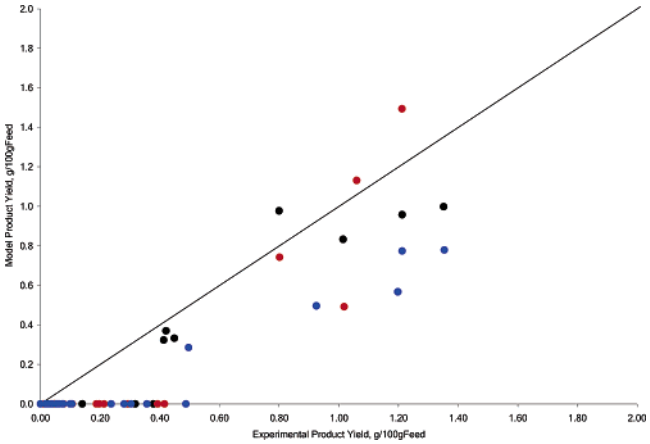

Figure 5. Parity plot for P5, P6, and P7 product yields.

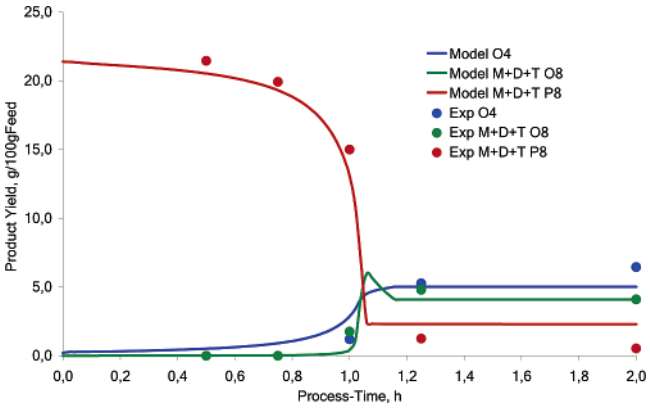

Figure 6. Evolution with process-time of exit product yields: temperature, 353 K; butene space-time (W/F°_{O4}), 0.24 h·gCat/mol; and isobutane/1-butene molar ratio, 7.7 mol/mol.

irreversibly adsorbed species are indeed reactive for other surface reactions.

Figure 7 presents the most relevant product-yield profiles along the reactor, i.e., versus the butene space-time, for a process-time of 0.5 h, when the downstream moving deactivation zone is halfway in the reactor. The selectivity shift from TP8 to DO8, like most of the transformations, occurs within the deactivation zone. The reactor is separated into two sections: one that extends from the reactor inlet to the onset of the deactivation zone and in which the deactivation is maximum and determined by the oligomerization/β-scission equilibrium, and a second one that extends from the moving deactivation

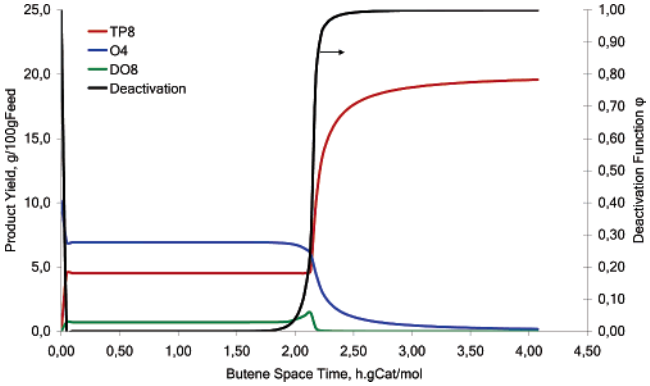

Figure 7. Product yields vs butene space-time: temperature, 373 K; butene space-time (W/F°_{O4}), 0.26 h·gCat/mol; and isobutane/1-butene molar ratio, 8.3 mol/mol; and process-time of 0.5 h.

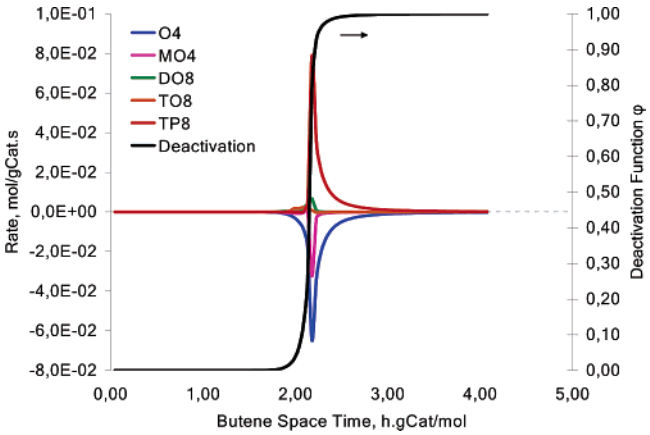

Figure 8. Moving deactivation zone; net production rates vs butene space-time: temperature, 373 K; total butene space-time (W/F°_{O4}), 0.26 h·gCat/mol; isobutane/1-butene molar ratio, 8.3 mol/mol; process-time, 0.5 h.

zone toward the reactor exit in which nondeactivated catalyst is available and most of the TP8 is formed.

The model also predicts profiles of net production rates along the reactor. Figure 8 reveals the role of isobutene (MO4) as a reaction intermediate with increasing deactivation. It leads to a selectivity shift from tribranched octanes to dibranched octenes. Within the first hour in process-time, as a consequence of PCP-branching deactivation, the experimentally observed selectivity shift turned out to be a result of the rapid disappearance of isobutene from the reaction mixture due to the decreasing formation of *tert*-butyl ions by hydride transfer with deactivation. Oligomerization of isobutene and linear butenes with *tert*-butyl ions leads to the formation of tribranched species.

Conclusions

A fundamental kinetic model at the elementary-step level was developed for the solid acid alkylation of isobutane with butenes over proton-exchanged Y-zeolites. A reduction in the number of model parameters from 3130 to 14 was accomplished by expressing the elementary-step rate coefficients in terms of the single-event concept, together with the application of the Evans−Polanyi relationship, the stabilization energy concept, and thermodynamic constraints on the rate expressions. Formulas for the calculation of symmetry numbers were derived from the identification of processes leading to the creation/destruction of symmetry axes and chiral centers in the formation of the transition-state structure. Additional contributions facilitating the application of the single-event approach were made with the introduction of the stabilization-energy dependency on

the carbenium-ion type and carbon number to account for the variations in the stabilization effect of the solid acid site. The paper presents further evidence for the power of the single-event approach in the kinetic modeling of complex processes.

The single-event model provides a rigorous treatment of the deactivation process through site coverage and predicts the observed rapid deactivation and nonzero steady conversion accompanied by shifts in the degree of saturation and branching of the reaction products. The prediction of the rate of deactivation caused by higher oligomers irreversibly linked to the catalyst sites and not detected at the exit of the reactor is possible only by expressing the kinetics in terms of single events. The rate of oligomerization is so fast that deactivation occurs in a narrow zone moving downstream toward the reactor exit. Deactivation is not observed at the exit of the reactor prior to breakthrough of this zone. Furthermore, the model also permitted us to identify the occurrence of oligomerization/β-scission equilibrium at the maximum deactivation level in the section preceding the moving deactivation zone. The evolution of this section with butene space-time until the exit of the reactor is reached leads to the nonzero steady-state conversion experimentally observed and to the selectivity shift from tribranched products to dibranched ones. Instead, the change in selectivity was attributed to the disappearance of isobutylene and *tert*-butyl ions with deactivation, which turn out to be intermediates in the formation of tribranched species along the oligomerization/β-scission reaction chain.

Finally, further research on solid acid alkylation should focus on the design of new materials with mesoporous structures and a high density of strong acid sites. Efforts can be made to decrease the energy of activation of the hydride-transfer elementary step so that this reaction could readily proceed with lower acid strength. Materials such as perfluorinated sulfonic acids supported on mesoporous silicas, where the distance between neighboring acid sites can be engineered to favor hydride-transfer steps, are strong candidates for further research.

Literature Cited

(1) Martinis, J. M.; Froment, G. F. Solid Acid Alkylation. Part 1. Experimental Investigation of Catalyst Deactivation. *Ind. Eng. Chem. Res*. **2006**, *45*, 940−953.

(2) Park, T.; Froment, G. F. Kinetic Modeling of the Methanol to Olefins Process. 2. Experimental Results, Model Discrimination, and Parameter Estimation. *Ind. Eng. Chem. Res*. **2001**, *40*, 4187.

(3) Alwahabi, S. M.; Froment, G. F. Single Event Kinetic Modeling of the Methanol-to-Olefins Process on SAPO-34. *Ind. Eng. Chem. Res*. **2004**, *43*, 5098.

(4) Nam, I.; Froment, G. F. Catalyst Deactivation by Site Coverage through Multi-Site Reaction Mechanisms. *J.Catal*. **1987**, *108*, 271.

(5) Denayer, J. F. M.; De Jonckheere, B.; Hloch, M.; Marin G. B.; Vanbutsele, G.; Martens, J. A.; Baron, G. V. Molecular Competition of C_7 and C_9 *n*-alkanes in Vapor- and Liquid-Phase Hydroconversion over Bifunctional Pt-USY Zeolite Catalysts. *J. Catal*. **2002**, *210*, 445.

(6) Kazansky, V. B. Adsorbed Carbocations as Transition States in Heterogeneous Acid-Catalyzed Transformations of Hydrocarbons. *Catal. Today* **1999**, *51*, 419.

(7) Clymans, P. J.; Froment, G. F. Computer-Generation of Reaction Paths and Rate Equations in the Thermal Cracking of Normal and Branched Paraffins. *Comput. Chem. Eng*. **1984**, *8-2*, 137.

(8) Vynckier E.; Froment, G. F. Modeling of the Kinetics of Complex Processes based upon Elementary Steps. In *Kinetic and Thermodynamic Lumping of Multicomponent Mixtures*; Astarita, G., Sandler, S. I., Eds.; Elsevier Science Publishers BV: Amsterdam, The Netherlands, 1984; p 131.

(9) Muller, C.; Scacchi, G.; Come, G. M. A Topological Method for Determining the External Symmetry Number of Molecules. *Comput Chem*. **1991**, *15* (1), 17.

(10) Walters, W. P.; Yalkowsky, S. H. ESCHER−A Computer Program for the Determination of External Rotational Symmetry Numbers from Molecular Topology. *J. Chem. Inf. Comput. Sci*. **1996**, *36*, 1015.

(11) Park, T.; Froment, G. F. Kinetic Modeling of the Methanol to Olefins Process. 1. Model Formulation. *Ind. Eng. Chem. Res*. **2001**, *40*, 4172.

(12) Dumesic, J. A.; Rudd, D. F.; Aparicio, L. M.; Rekoske, J. E.; Treviño, A. A. *The Microkinetics of Heterogeneous Catalysis*; American Chemical Society: Washington, DC, 1993.

(13) Evans, M. G.; Polanyi, M. Inertia and Driving Force of Chemical Reactions. *Trans. Faraday Soc*. **1938**, *31*, 11.

(14) Alwahabi, S. M.; Froment, G. F. Single Event Kinetic Modeling of the Methanol-to-Olefins Process on SAPO-34. *Ind. Eng. Chem. Res*. **2004**, *43*, 5098.

(15) Benson, S. W. *Thermochemical Kinetics*; Wiley: New York, 1968.

(16) Linstrom, P. J., Mallard, W. G., Eds. *NIST Chemistry WebBook*; NIST Standard Reference Database Number 69; National Institute of Standards and Technology: Gaithersburg, MD, 2003 (http://webbook.nist.gov).

(17) Park, T. Kinetic Modeling of MTO Process. Ph.D. Dissertation, Universiteit Gent, Belgium, 1998.

(18) Rùzicka, V.; Domalski, E. S. Estimation of the Heat Capacities of Organic Liquids as a Function of Temperature using Group Additivity. I. Hydrocarbon Compounds. *J. Phys. Chem. Ref. Data* **1993**, *22*, 597.

(19) Constantinou, L.; Gani, R. New Group Contribution Method for Estimating Properties of Pure Compounds. *AIChE J*. **1994**, *40*, 1697.

(20) Shampine, L. F.; Reichelt, M. W. The MATLAB ODE Suite. *SIAM J. Sci. Comput*. **1997**, *18*, 1.

(21) Froment, G. F.; Bischoff, K. B. *Chemical Reactor Analysis and Design*, 2nd ed.; Wiley: New York, 1990.

(22) Grace, A. *MATLAB Optimization Toolbox User's Guide*; The Math Works, Inc.: Natick, MA, 1994.

(23) Gallant, A. R. Nonlinear Regression. *Am. Stat*. **1975**, *29*, 73.

Received for review August 4, 2005
Revised manuscript received October 13, 2005
Accepted October 17, 2005

IE050910V